Coupling between a Weyl semimetal and a nontopological metal

L. Goutte* and T. Pereg-Barnea
Department of Physics and Centre for the Physics of Materials, McGill University, Montréal, Québec, Canada H3A 2T8

(Received 13 January 2023; accepted 29 June 2023; published 11 July 2023)

We study the effects of tunneling between a Weyl semimetal (WSM) and a simple parabolic band. When coupled to the nonmagnetic parabolic band, the interface between the two exhibits two main phenomena. First, the WSM's chiral arc state lowers in energy, and second, a previously extended WSM state becomes localized to the interface and is lowered in energy. Together these surface bound states create a new closed orbit in momentum space, and a noticeable spin-dependent asymmetry in the interface spectrum in the vicinity of the Weyl nodes appears. We study these effects with a lattice model that we solve numerically on a finite sample and analytically using an *Ansatz* on an infinite sample. Our *Ansatz* agrees very well with the numerical simulation as it accurately describes the behavior of the chiral state, from its energy asymmetry to the spin rotation at the interface. We find that the tunneling effectively increases the Fermi arc length, allowing for the presence of interface states beyond the bare Weyl nodes. These additional states may carry current along the interface, and their contribution can be detected in the conductance. In addition to conductivity, the effect of tunneling between the WSM and the metal can be seen in quantum oscillation experiments, which we briefly address.

DOI: 10.1103/PhysRevB.108.035118

I. INTRODUCTION

Weyl semimetals (WSMs) are materials whose low-energy excitations are Weyl fermions due to band crossing at the Fermi level [1–3]. While these particles have been initially predicted in high-energy physics as solutions to the massless three-dimensional Dirac equation with definite chirality, WSMs present a way of realizing them in condensed-matter settings. A growing interest in these materials culminated with their physical realization in TaAs [4,5], NbAs [6], and $Co_3Sn_2S_2$ [7], with additional predictions of type-II WSMs in WTe_2 [8] and $MoTe_2$ [9]. On the theoretical side, the classification of WSMs as a gapless topological phase makes them an appealing object of study with deep connections to topological Chern insulators [10] and novel properties in the presence of external magnetic fields [11], to name but a few.

The Weyl Hamiltonian describes a linear crossing of two nondegenerate bands. For a pair of such bands to touch, one must in general tune three independent parameters, one for each Pauli matrix [1,12]. In three spatial dimensions with three independent momenta, these band crossings, so-called Weyl nodes, are therefore robust against weak perturbations. Near these nodes, the bulk energy disperses linearly and the physics are governed by the Weyl Hamiltonian

$$H = \hbar \mathbf{v}_0 \cdot \mathbf{k} \pm \hbar v \mathbf{k} \cdot \boldsymbol{\sigma}, \tag{1}$$

where $\pm$ denotes the node's chirality, v is the effective Fermi velocity, $\mathbf{k}$ is the momentum, and σ is a vector of Pauli matrices acting in spin space. The first term, proportional to the unit matrix, breaks Lorentz invariance and tilts the dispersion. For type-I WSMs it can be ignored, leaving only the second term. The latter has a linear dispersion that, while strongly reminiscent of two-dimensional (2D) graphene, will not open a gap in the presence of small perturbations. Each Weyl node is also a monopole of Berry curvature, leading to a chiral anomaly that manifests itself in a negative magnetoresistance [13], for instance.

In lattice systems, a Weyl semimetal hosts pairs of Weyl nodes of opposite chirality [14–16] along a given nodal direction [1,17,18]. This is required by either time-reversal ($\mathcal{T}$) or inversion ($\mathcal{I}$) symmetry and the fact that the total Berry flux in the first Brillouin zone (BZ) must vanish. Consequently, if one imagines creating a momentum space slice of our WSM model, such that the momentum in the direction of the Weyl node separation, k_z, is fixed, then each of the resulting 2D models can be characterized by a Chern number. When varying k_z, the Chern number changes by ± 1 at the Weyl point, representing a transition between a Chern insulator and a trivial one [19,20]. Therefore, the bulk-boundary correspondence implies the presence of topologically protected surface states residing on an arc in the surface momentum space. The arc begins and ends at the projection of the Weyl nodes on the surface momentum. The arc states are chiral as they connect the Weyl nodes that serve as a source and drain of Berry curvature. The surface states disperse linearly away from the Fermi level [21]. In this sense, gapless topological phases are intermediaries between genuine trivial and topological phases of matter, and they can even be realized by a repeated stacking of the two [18].

Recently, much work has been done to understand how WSM surface states change when put into contact with a nontopological material (see, e.g., Refs. [22–26]). Among many potential applications, these Fermi arcs may be utilized to mitigate grain boundary scattering [27], and so it is crucial to understand how they behave when put in contact with other

*leo.goutte@mail.mcgill.ca

systems. In what follows, we approach this problem by constructing a simple tight-binding model of a time-reversal ($\mathcal{T}$) broken WSM coupled to a nonmagnetic band over two lattice sites. We choose a model with broken time reversal such that only two Weyl points are present while all the aforementioned properties can be studied without further complication. Generalization to time-reversal-invariant models with more Weyl points can be easily done. Likewise, our choice of a simple tunneling potential and featureless band is intentional: We seek to draw out the bare properties of a WSM in contact with a nontopological material.

The remaining sections are structured as follows. In Sec. II, we present the WSM and nonmagnetic band models along with the specific form of surface tunneling. The numerical results of a finite lattice model are then presented in Sec. III. In Sec. IV, we derive an infinite lattice theory with an interface to model the spectra, spin rotation, and interface arcs in a lattice framework, while Sec. V presents a simpler continuum model. We finish in Sec. VI by investigating the novel transport properties of the coupled system both along and across the interface in the Landauer-Büttiker and electron tunneling formalism, respectively. Directions for further study are briefly touched upon in the conclusion, Sec. VII, and relevant technical details are included in the Appendixes.

II. MODEL

A. Weyl semimetal

We consider a minimal Hamiltonian that captures the Fermi arc feature. This can be achieved either by breaking time reversal, $\mathcal{T}$, while preserving inversion, $\mathcal{I}$, or vice-versa. To work with smaller matrices, we choose the former. Explicitly, our bulk Hamiltonian must satisfy $H(\mathbf{k}) = \sigma_z H(-\mathbf{k})\sigma_z$ and $H(\mathbf{k}) \neq \sigma_y H^*(-\mathbf{k})\sigma_y$. A simple tight-binding Hamiltonian that abides by these symmetries is ($\hbar =$ lattice constant $= 1$) [1]

$$H_w = \sum_{\mathbf{k}} \mathbf{c}_{\mathbf{k}}^\dagger \mathcal{H}_w^{\text{bulk}}(\mathbf{k}) \mathbf{c}_{\mathbf{k}}, \tag{2a}$$

$$\mathcal{H}_w^{\text{bulk}}(\mathbf{k}) = t \sin k_x \sigma_x + t \sin k_y \sigma_y + t m(\mathbf{k}) \sigma_z, \tag{2b}$$

$$m(\mathbf{k}) = (2 + \gamma - \cos k_x - \cos k_y - \cos k_z). \tag{2c}$$

Here, $\mathbf{c}_{\mathbf{k}} = (c_{\mathbf{k},\uparrow}, c_{\mathbf{k},\downarrow})^\top$ is an annihilation operator in momentum space, t is the strength of hopping, and σ are the Pauli spin matrices. Note that σ may represent a pseudospin and not necessarily a physical spin. The Hamiltonian (2) admits the bulk energies

$$E_\pm = \pm t[\sin^2 k_x + \sin^2 k_y + m^2(\mathbf{k})]^{\frac{1}{2}}. \tag{3}$$

These vanish at $\mathbf{k}_w^\pm = (0, 0, \pm \arccos \gamma) \equiv (0, 0, \pm k_w)$—the aforementioned Weyl nodes. We emphasize the importance of the $\cos k_{x,y}$ terms, without which there could be more than two Weyl points in the BZ for a given γ.

These gapless bulk momenta $\mathbf{k}_w^\pm$ suggest that H_w exhibits different phases that depend solely on the arc length parameter γ. For $\gamma > 1$, $m(\mathbf{k}) > 0$ for all $\mathbf{k}$ and the system is trivially gapped. As γ decreases to 1, a pair of Weyl nodes appear at the origin and move outward along k_z as γ decreases further. This defines a gapless topological phase whereby a nonzero Berry flux flows within the momentum range $|k_z| < k_w$ from the node of negative chirality to that of positive chirality. If one imagines dividing the system into two-dimensional slices of fixed k_z, then each slice can be characterized by a Chern number. The Chern number is nonzero between the nodes, and zero beyond them. When $\gamma \leqslant -1$, the Weyl nodes reach the BZ boundaries and disappear, leaving the bulk dispersion with an inverted band gap. Between $-5 < \gamma < -1$, the same process occurs for Weyl nodes with $(k_x, k_y) = (0, \pi)$, $(\pi, 0)$, and (π, π), until $\gamma < -5$, where the system is again gapped and trivial for all $\mathbf{k}$. In all numerical results that follow, we take $\gamma = 0$ (such that $k_w = \pi/2$), well within the gapless topological regime and with a Fermi arc length $k_{\text{arc}} = \pi$. The bare WSM's surface spectrum, Fermi arc, and topological phases are shown in Fig. 1.

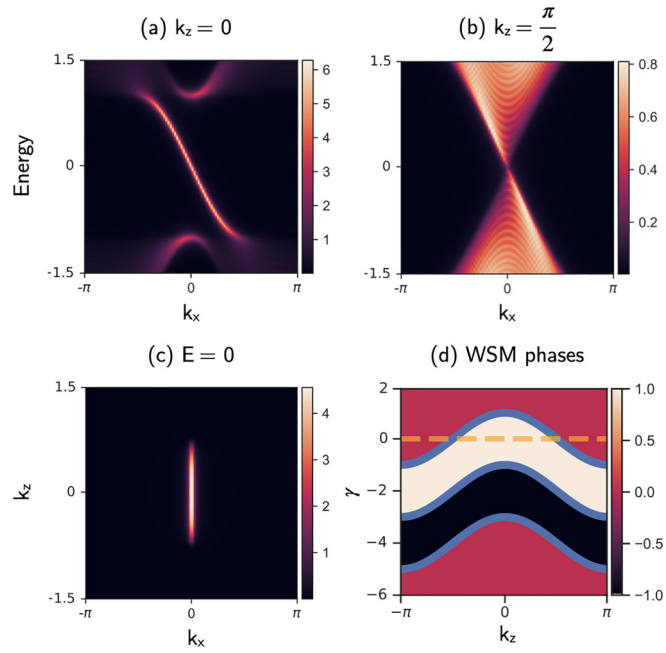

FIG. 1. The minimal Weyl semimetal model. (a) Spectral function at the sample surface, $y = L_y - 1$, of a WSM with open boundary conditions in y plotted in the $E - k_x$ plane for fixed $k_z = 0$ and (b) $k_z = \pi/2$. (c) WSM spectral function plotted in the $k_x - k_z$ plane for fixed $E = 0$ showing the Fermi arc. (d) Phase diagram of Eq. (2) where k_z is fixed and the two other directions are analyzed as a 2D system. The color represents the lower band's Chern numbers. The phase boundaries $\gamma = \cos k_z$, $\gamma = \cos k_z - 2$, and $\gamma = \cos k_z - 4$ are marked in blue. We will work at $\gamma = 0$ (dashed orange line).

B. Tunneling

To draw out the tunneling properties of the Weyl semimetal, we couple it to a simple parabolic band via spin-independent hopping between the WSM surface atoms and their nearest neighbor on the parabolic band. The band's Hamiltonian is spin-independent and reads

$$H_m = \sum_{\mathbf{k}} \mathbf{d}_{\mathbf{k}}^\dagger \mathcal{H}_m^{\text{bulk}}(\mathbf{k}) \mathbf{d}_{\mathbf{k}}, \tag{4a}$$

$$\mathcal{H}_m^{\text{bulk}}(\mathbf{k}) = -2t_m(\cos k_x + \cos k_y + \cos k_z) - \mu, \tag{4b}$$

where t_m is the hopping amplitude, μ is the chemical potential, and $\mathbf{d}_{\mathbf{k}} = (d_{\mathbf{k},\uparrow}, d_{\mathbf{k},\downarrow})^\top$ is an annihilation operator in

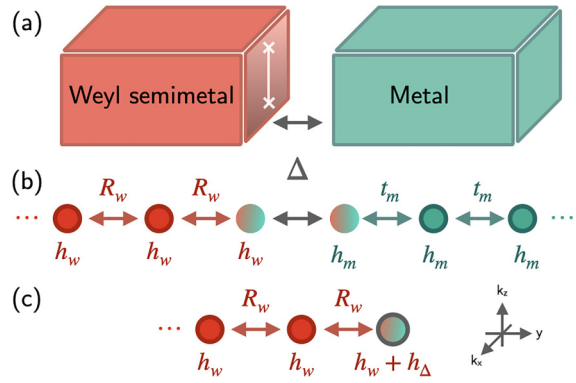

FIG. 2. (a) Schematic of the WSM-metal system. Only the rightmost surface, or *interface* (with the Fermi arc shown as a white line and the nodes as white crosses), is linked to the metal via tunneling Δ. (b) Physical representation of the system as a chain ($\mathbf{R}_w$, $\mathbf{h}_w$, etc. defined in Appendix A). (c) By integrating out the metal degrees of freedom, the chain is simplified into a single semi-infinite chain with a single edge site with an energy shift $h_\Delta = T^\dagger G_m T$ (shaded with a gray line).

momentum space. For brevity, we equivalently refer to this nonmagnetic parabolic band as "metal", though one may of course tune μ to achieve a semiconductor or an insulator, as discussed in Appendix B, where we also consider two parabolic bands.

We now introduce a tunneling Hamiltonian that couples the surface of the WSM to the surface of the metal. We proceed with open boundary conditions in the y-direction and keep well-defined momenta perpendicular to the surface, $\mathbf{k}_\perp = (k_x, k_z)$. The WSM (metal) side runs from $y = -L_y + 1$ to 0 ($y = 1$ to L_y), defining an interface between the WSM's $y = 0$ and metal's $y = 1$ sites. The Hamiltonian for the full (finite-sized) system is therefore

$$H = \sum_{\mathbf{k}_\perp} \sum_{y,y'=-L_y+1}^{L_y} \mathbf{f}^\dagger_{\mathbf{k}_\perp,y} \mathcal{H}(\mathbf{k}_\perp)_{y,y'} \mathbf{f}_{\mathbf{k}_\perp,y'}, \tag{5a}$$

$$\mathcal{H}(\mathbf{k}_\perp) = \begin{pmatrix} \mathcal{H}^{\text{open}}_w(\mathbf{k}_\perp) & T^\dagger \\ T & \mathcal{H}^{\text{open}}_m(\mathbf{k}_\perp) \end{pmatrix}, \tag{5b}$$

where

$$\mathbf{f}_{\mathbf{k}_\perp,y} = \begin{cases} \mathbf{c}_{\mathbf{k}_\perp,y}, & -L_y + 1 \leqslant y \leqslant 0, \\ \mathbf{d}_{\mathbf{k}_\perp,y}, & 1 \leqslant y \leqslant L_y, \end{cases} \tag{6}$$

and $\mathcal{H}^{\text{open}}$ is the partial-in-y Fourier transform of $\mathcal{H}^{\text{bulk}}$. The full form of Eq. (5) is shown in Appendix A. The surface tunneling term takes the form

$$(T)_{y,y'} = \Delta \delta_{0,L_y-1}, \tag{7}$$

where, for simplicity, we have assumed that Δ is a real constant representing the tunneling strength.[1] Physically, the tunneling strength can be modified either by varying the metal bandwidth t_m or by changing the interface thickness, as suggested by Fig. 2. There are therefore two competing energy scales at the WSM's interface: The interlayer hopping t pulling the electron towards the bulk, and the tunneling strength Δ pulling the electron towards the metal.

Before moving on to the numerical results of our model on a finite lattice, we note that the metal degrees of freedom can be integrated out to make way for an effective WSM propagator [28,29]. More precisely, the effective Green's function becomes

$$G_{\text{eff}}(i\omega_n) = \left[G_w^{-1}(i\omega_n) - T^\dagger G_m(i\omega_n) T\right]^{-1}, \tag{8}$$

where ω_n is the Matsubara frequency, and $G_{w,m} = (i\omega_n - \mathcal{H}^{\text{open}}_{w,m})^{-1}$ are the bare Green's functions. Substituting in Eqs. (4) and (7) yields

$$T^\dagger G_m(i\omega_n) T = -\frac{\Delta^2}{\sqrt{(i\omega_n - h_m)^2 - 4t_m^2}} \delta_{y,L_y-1}\delta_{y,y'}, \tag{9}$$

where $h_m = -2t_m(\cos k_x + \cos k_z) - \mu$. Surface tunneling simply shifts the same-site hopping of the last site [Fig. 2(c)].

III. FINITE LATTICE MODEL

We now turn to the numerical results of Eq. (5) on a finite lattice. Keeping the system open in y with the quantum numbers k_x and k_z, we calculate the Green's function, defined by

$$G(E, \mathbf{k}_\perp) = [E + i0^+ - \mathcal{H}(\mathbf{k}_\perp)]^{-1}, \tag{10}$$

and the spectral function, $A(E, \mathbf{k}_\perp) = -\pi^{-1}\text{Im}[\text{Tr}(G)]$. The interface spectral function displayed in Fig. 3 is found by tracing over the $y = 0$ site only.

At $k_z = 0$ [Fig. 3(a)], we are exactly in between the Weyl nodes. Without tunneling, only the Fermi arc state is present and localized to the interface, residing on the Fermi arc and dispersing as $E = -t \sin k_x$ with a spin $\sigma_x = -1$. With tunneling, there are two noticeable effects. First, the chiral Fermi arc state (which will henceforth be referred to as a *chiral state*) is lowered in energy. This is due to the possibility to spread the wave function wider into the metal side. This lowering of energy captured by Eqs. (8) and (9) is a prevailing effect throughout this work. Second, a previously extended state enters the bulk gap from the upper bulk band and localizes to the interface. Contrary to the chiral state, this so-called *emergent interface state* does not have a uniform spin polarization.

At the Weyl nodes [Fig. 3(b)], the Fermi arc terminates and there are no interface states for $\Delta = 0$. As tunneling is increased, however, the chiral state can be seen along the Weyl node's upper cone. When Δ increases beyond the interlayer hopping t, the chiral state detaches from the Weyl cone and forms, together with the emergent interface state, a noticeable asymmetry in the spectral function at the interface with respect to k_x reflection [Fig. 3(b.iii)]. This striking asymmetry is of particular interest. Physically, it suggests that tunneling modifies the group velocity along the interface to produce additional left- and right-flowing current in an energy range between the chiral and emergent interface states' intersections with the bulk dispersion. Naively, this is surprising because one may not expect the breaking of translation symmetry in

[1] A more realistic tunneling, e.g., one that extends over multiple metal sites, can always be effectively recast as a strong localized tunneling via the procedure outlined in Sec. II B.

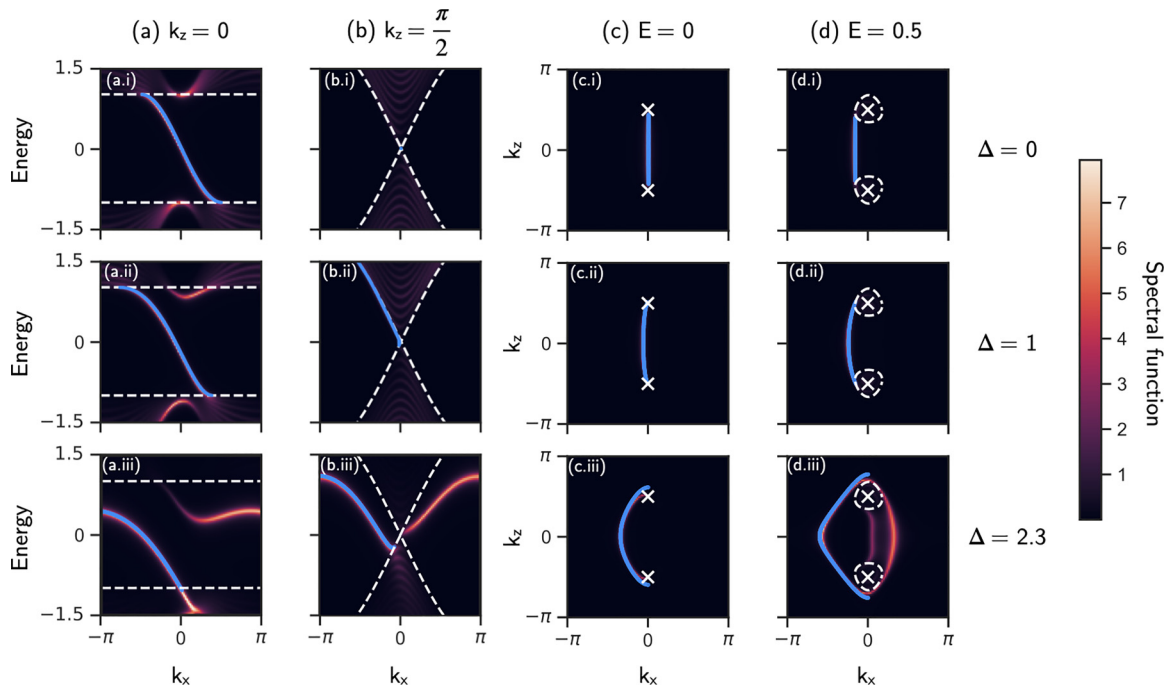

FIG. 3. Spectral function at the interface for the coupled WSM-metal system for both spins. The numerical results (simulated on an $L_y = 30$ sized chain sampled at 100 momentum points) are shown in warm colors, whereas the chiral state's infinite lattice model (Sec. IV) is plotted in blue. In all plots where the infinite lattice theory obstructs the numerical results (e.g., the top left), the agreement is near exact. The columns correspond to (a) the spectrum along k_x at $k_z = 0$, (b) the spectrum along k_x at the Weyl point $k_z = +\pi/2$, and the emergent interface arcs at (c) $E = 0$ and (d) $E = 0.5$. The rows are set in increasing order of $\Delta = 0$, 1, 2.3 going down. The bulk energy edges $E_{\text{bulk}} = \pm t[\sin^2 k_x + (1 + \gamma - \cos k_x - \cos k_z)^2]^{\frac{1}{2}}$ are denoted by dashed white lines, as is the Fermi surface in the $E = 0.5$ interface plots. The bare Weyl nodes $\mathbf{k}^{\pm}_{\perp,w} = (0, \pm\pi/2)$ are white crosses. The fixed parameters used for these and all other plots are $t = 1$, $\gamma = 0$, $t_m = 0.5$, $\mu = -4$, unless otherwise specified.

y to induce an asymmetry in the x-direction. However, one must remember that the physics on a single surface are not in fact symmetric in k_x to begin with, as evidenced by the linearly dispersing chiral state at the interface. Therefore, although the spectral function is symmetric in k_x when traced over all sites, the localized tunneling term in y will explicitly break this symmetry.

By plotting $A(E, \mathbf{k}_\perp)$ in the surface BZ, we see that the zero-energy interface Fermi arc [Figs. 3(c) and 3(d)] will curve in the presence of tunneling [30]. While still terminating at the Weyl nodes $\mathbf{k}^{\pm}_{\perp,w} = (0, \pm k_w)$, it does go beyond $k_z = \pm k_w$ at zero energy due to this curving, thereby signifying the existence of interface states in a region of parameters outside the bare Fermi arc. This is illustrated by the chiral state's presence at $k_z = \pi/2$ and will have important transport consequences starting in Sec. VI.

These results are robust to changes in the metal's dispersion relation. In fact, we find that equivalent behavior may be obtained simply by coupling the WSM to a constant energy reservoir $t_m = 0$, $\mu = -M$. A more realistic setup in which the WSM is coupled to a two-band bulk insulator will yield two copies of the dispersion found in Fig. 3, one for positive and one for negative energy (see Appendix B).

Finally, as seen in the numerics above, a new closed orbit of low-energy states appears on the interface. This closed orbit should be apparent in quantum oscillation experiments as it leads to oscillations with frequency, which matches the enclosed momentum space area. These oscillations should be contrasted to the arc/node oscillations suggested by Ref. [31] and studied in Ref. [28]. The latter oscillations result from closed orbits, which include both the surface (interface) and bulk states, meaning their frequency depends on the slab depth. By contrast, the new orbit seen in Fig. 3(d.iii) contains only interface states, and its frequency is depth-independent. We leave the study of these orbits open for future work.

IV. INFINITE LATTICE THEORY WITH AN INTERFACE

The physics at the interface seen in the lattice model above can be described in an infinite model and treated analytically with the help of an *Ansatz*. We take $L_y \to \infty$ and impose $\psi \to 0$ at $y \to \pm\infty$ on both sides of the interface. Therefore, this theory effectively consists of two semi-infinite slabs connected by surface tunneling Δ.

To simplify the algebra, we perform a unitary transformation $U = \frac{1}{\sqrt{2}}(1 - i\sigma_y)$. In the next sections, we will use the following definitions:

$$g_1 = t \sin k_x, \tag{11a}$$

$$g_3 = t(2 + \gamma - \cos k_x - \cos k_z), \tag{11b}$$

$$\mathbf{h}_w = g_1\sigma_z - g_3\sigma_x, \tag{11c}$$

$$\mathbf{R}_w = \frac{t}{2}(\sigma_x + i\sigma_y), \tag{11d}$$

where $\mathbf{h}_w$ contains all in-plane terms and $\mathbf{R}_w$ represents the nearest-neighbor hopping along the y axis. $\mathbf{h}_w$ and $\mathbf{R}_w$ are matrices in spin space.

A. $\Delta = 0$

As a first test of validity, we take the $\Delta = 0$ case and recover the chiral state and Fermi arc of the finite lattice model. In a lattice formalism, $\mathcal{H}_w^{\text{open}}\boldsymbol{\varphi}_w = E\boldsymbol{\varphi}_w$ produces a set of coupled difference equations relating $\boldsymbol{\varphi}_w(y)$ to its nearest neighbors $\boldsymbol{\varphi}_w(y \pm 1)$ [32]. Without the possibility of tunneling into the metal, there are two distinct equations, one for the bulk (hopping to both $y+1$ and $y-1$) and one for the interface (hopping to $y=-1$ only). They read

$$E\boldsymbol{\varphi}(y) = \mathbf{h}_w\boldsymbol{\varphi}(y) + \mathbf{R}_w^\dagger\boldsymbol{\varphi}(y+1) + \mathbf{R}_w\boldsymbol{\varphi}(y-1) \tag{12a}$$

and

$$E\boldsymbol{\varphi}(0) = \mathbf{h}_w\boldsymbol{\varphi}(0) + \mathbf{R}_w\boldsymbol{\varphi}(-1), \tag{12b}$$

respectively. Seeking states $\boldsymbol{\varphi}$ exponentially localized to the interface, we make the *Ansatz*

$$\boldsymbol{\varphi} \propto \begin{cases} e^{ik_x x + ik_z z}\ell^y\boldsymbol{\phi}_w, & y = -\infty, \ldots, -1, 0, \\ e^{ik_x x + ik_z z}\ell_m^{-y+1}\boldsymbol{\phi}_m, & y = 1, 2, \ldots, \infty, \end{cases} \tag{13}$$

where $\boldsymbol{\phi}_{w,m}$ are spinors. Note that this *Ansatz* assumes a constant spin direction and is therefore suitable for the chiral state found above but is not completely general. Plugging in Eq. (13), we obtain the matrix equations

$$(E - g_1\sigma_z + g_3\sigma_x - t\ell^{-1}\sigma_+ - t\ell\sigma_-)\boldsymbol{\phi}_w = 0, \tag{14a}$$

$$(E - g_1\sigma_z + g_3\sigma_x - t\ell^{-1}\sigma_+)\boldsymbol{\phi}_w = 0, \tag{14b}$$

where $\sigma_\pm = \frac{1}{2}(\sigma_x \pm i\sigma_y)$. Subtracting Eq. (14b) from Eq. (14a) reveals the condition

$$t\ell\sigma_-\boldsymbol{\phi}_w = 0 \tag{15}$$

for the chiral state. Clearly, the factor ℓ, which represents the spatial decay into the bulk, is nonzero for a surface state. Therefore, the chiral state is an eigenstate of σ_x with eigenvalue -1. Setting the determinant of Eq. (14a) to zero yields the ratio of spins and the energy, respectively,

$$\frac{\phi_w^\uparrow}{\phi_w^\downarrow} = \frac{E + g_1}{t\ell - g_3} = \frac{t\ell^{-1} - g_3}{E - g_1}, \tag{16a}$$

$$E = \pm\left[g_1^2 + g_3^2 + t^2 - g_3 t(\ell + \ell^{-1})\right]^{\frac{1}{2}}, \tag{16b}$$

where $\pm$ is the band index. Setting $\phi_w^\uparrow/\phi_w^\downarrow = 0$ for a state with spin in the $-x$ direction, we find $\ell = t/g_3$ and $E = -g_1$ for the chiral state.

To satisfy the boundary condition at $y \to -\infty$, we impose $\mathrm{Re}(\ell) > 1$, or $|g_3| < t$. The familiar Fermi arc condition $\gamma < \cos k_z$ then follows naturally.[2] We have therefore recovered the aforementioned chiral state: A unidirectional interface state on the Fermi arc.

[2]For a bulk state of energy E, $\mathrm{Re}(\ell) > 1$ implies $-E_{\text{bulk}} < E < E_{\text{bulk}}$, where $E_{\text{bulk}}(\mathbf{k}_\perp) = [g_1^2 + (g_3 - t)^2]^{\frac{1}{2}}$ is the bulk edge.

B. $\Delta > 0$

We now allow for tunneling at the interface between the $y = 0$ and 1 sites. There are then four difference equations, one for each type of site: The Weyl bulk, Weyl interface, metal interface, and metal bulk. Substituting in the supposed form of $\boldsymbol{\varphi}$, the difference equations are, respectively,

$$(E - g_1\sigma_z + g_3\sigma_x - t\ell\sigma_- - t\ell^{-1}\sigma_+)\boldsymbol{\phi}_w = 0, \tag{17a}$$

$$(E - g_1\sigma_z + g_3\sigma_x - t\ell^{-1}\sigma_+)\boldsymbol{\phi}_w - \Delta\boldsymbol{\phi}_m = 0, \tag{17b}$$

$$\left(E - h_m + t_m\ell_m^{-1}\right)\boldsymbol{\phi}_m - \Delta\boldsymbol{\phi}_w = 0, \tag{17c}$$

$$\left(E - h_m + t_m\ell_m^{-1} + t_m\ell_m\right)\boldsymbol{\phi}_m = 0. \tag{17d}$$

Equation (17c) has no matrix structure and is hence the same for both components of the spinor, requiring the spinor direction to be the same on both sides of the interface. Moreover, it determines the magnitude ratio

$$\boldsymbol{\phi}_m = \frac{\Delta}{E - h_m + t_m\ell_m^{-1}}\boldsymbol{\phi}_w. \tag{18}$$

Together with Eq. (17b), we obtain

$$\left(E - \frac{\Delta^2}{E - h_m + t_m\ell_m^{-1}} - g_1\sigma_z + g_3\sigma_x - t\ell^{-1}\sigma_+\right)\boldsymbol{\phi}_w = 0. \tag{19}$$

Equation (19) is similar in form and purpose to the effective surface Green's function (8) except it is purely in spin space since the *Ansätze* and vanishing boundary conditions took care of position dependencies. It can be interpreted as an eigenvalue problem for the matrix $g_1\sigma_z - g_3\sigma_x + \ell^{-1}\sigma_+$, whose eigenvalues are

$$E_\Delta \equiv E - \frac{\Delta^2}{E - h_m + t_m\ell_m^{-1}}. \tag{20}$$

With this, its energy bands are twofold and defined by the implicit equation

$$E - \frac{\Delta^2}{E - h_m + t_m\ell_m^{-1}} = \pm\left(g_1^2 + g_3^2 - tg_3\ell^{-1}\right)^{\frac{1}{2}}, \tag{21}$$

where ℓ and ℓ_m are themselves functions of the energy, which are found by requiring that the determinant of the right-hand side of Eqs. (17a) and (17d) vanishes:

$$\ell_\pm = Q \pm \sqrt{Q^2 - 1}, \tag{22a}$$

$$\ell_{m,\pm} = P \pm \sqrt{P^2 - 1}. \tag{22b}$$

Here, $Q = \frac{g_1^2 + g_3^2 + t^2 - E^2}{2g_3 t}$ and $P = \frac{h_m - E}{2t_m}$. While it may seem at first glance that the energies are symmetric in k_x due to the even parity of both ℓ and ℓ_m with respect to k_x, one must be careful in choosing the appropriate branch, such that the state indeed decays away from the interface. In general, the branch may vary as a function of $\mathbf{k}_\perp$.

The energies obtained from Eq. (21) agree with the shape of the numerical results obtained in Sec. III, albeit with noticeable discrepancies. The problem is that our system is overconstrained. Indeed, there are a total of nine equations [Eq. (17) and normalization] and eight variables (the two components of each $\boldsymbol{\phi}_w$ and $\boldsymbol{\phi}_m$, ℓ, ℓ_m, E, and normalization). We find that a better expression of the energy can be obtained

by relaxing the initial *Ansatz* to allow the spin at the zeroth site, $\boldsymbol{\phi}_w^0$, to differ from the spin in the remainder of the WSM:

$$\boldsymbol{\varphi}_{\text{mod}} \propto \begin{cases} e^{ik_x x + ik_z z}\ell^y \boldsymbol{\phi}_w, & y = -\infty, \ldots, -1, \\ e^{ik_x x + ik_z z}\boldsymbol{\phi}_w^0, & y = 0, \\ e^{ik_x x + ik_z z}\ell_m^{-y+1}\boldsymbol{\phi}_m, & y = 1, 2, \ldots, \infty. \end{cases} \tag{23}$$

There are now five difference equations, one for each type of site: The Weyl bulk, Weyl $y = -1$ site, Weyl interface, metal interface, and metal bulk. The Weyl and metal bulk equations remain unchanged. The Weyl and metal bulk equations are still Eqs. (17a) and (17d), respectively. The Weyl $y = -1$, Weyl interface, and metal interface equations are

$$(E - g_1\sigma_z + g_3\sigma_x - t\ell^{-1}\sigma_+)\boldsymbol{\phi}_w - t\ell\sigma_-\boldsymbol{\phi}_w^0 = 0, \tag{24a}$$

$$(E - g_1\sigma_z + g_3\sigma_x)\boldsymbol{\phi}_w^0 - t\ell^{-1}\sigma_+\boldsymbol{\phi}_w - \Delta\boldsymbol{\phi}_m = 0, \tag{24b}$$

$$\left(E - h_m + t_m\ell_m^{-1}\right)\boldsymbol{\phi}_m - \Delta\boldsymbol{\phi}_w^0 = 0, \tag{24c}$$

respectively. Using Eq. (24a) to relate $\boldsymbol{\phi}_w$ to $\boldsymbol{\phi}_w^0$ and Eq. (24c) to relate $\boldsymbol{\phi}_m$ to $\boldsymbol{\phi}_w^0$, we arrive at the matrix equation

$$\left(E_\Delta - \frac{E - g_1}{2D}(1 + \sigma_z) - g_1\sigma_z + g_3\sigma_x\right)\boldsymbol{\phi}_w^0 = 0, \tag{25}$$

where $D = \frac{E^2 - g_1^2 - g_3^2 + g_3 t/\ell}{t^2}$. Requiring that the matrix be singular yields

$$E_\Delta - \frac{E - g_1}{2D} = \pm\left[g_3^2 + \left(g_1 + \frac{E - g_1}{2D}\right)^2\right]^{\frac{1}{2}}, \tag{26}$$

which can be implicitly solved for E. The infinite lattice theory Eq. (26) is found to be in very good agreement with the finite lattice model, as seen in Fig. 3.

A perfect description of the finite lattice model would necessitate an *Ansatz* with a potentially distinct spin on every site. Since the chiral state has most of its weight on the interface, our approximation of only allowing the $y = 0$ site to differ from the remaining WSM sites is a fine and physically justified one. What we gain in quantitative accuracy, however, we lose in intuition, as Eqs. (25) and (26) do not have the same pleasant interpretation as Eqs. (19) and (21).

Another remarkable consequence of tunneling is spin rotation. At first glance, one should not expect that nonmagnetic tunneling to a nonmagnetic metal should cause the polarized spins at the interface to rotate away from the $-x$ direction (which was found in the previous section). Indeed, this intuition is supported by Eq. (18) and in fact agrees with the finite lattice model for $\Delta \lesssim t$. To paint a more complete picture, however, we must consider the ratio of spins of the interface state, which, in light of Eq. (25), is

$$\frac{\phi_w^\uparrow}{\phi_w^\downarrow} = \frac{E_\Delta + g_1}{-g_3}. \tag{27}$$

For $\Delta > 0$ and if $E < h_m + t_m\ell_m^{-1}$, we expect the interface spin to rotate away from $\phi_w^\uparrow/\phi_w^\downarrow = 0$ ($\sigma_x = -1$ in the original basis) towards $\phi_w^\uparrow/\phi_w^\downarrow = -1$ ($\sigma_z = +1$ in the original basis) due to the energy lowering brought on by Δ. Solving for $\phi_w^\uparrow/\phi_w^\downarrow$ together with Eq. (26) yields the spins at the interface of the chiral state as they vary with tunneling, shown in Fig. 4, panel (a). We therefore conclude that nonmagnetic surface tunneling to a nonmagnetic band can in fact induce a change in the spins of the WSM's chiral states. The spin rotation is related to the curvature of the Fermi arc, as seen in Fig. 4, panel (b).

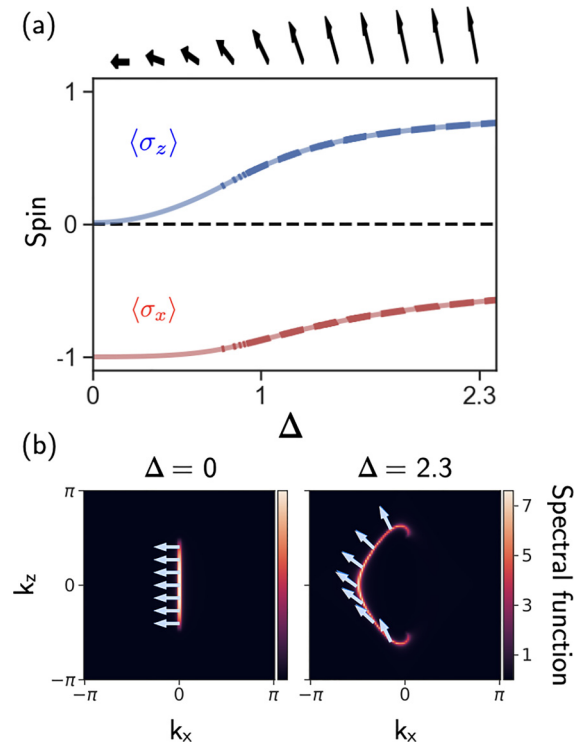

FIG. 4. (a) The chiral state's spin at the interface, fixed at the Weyl node $k_z = \pi/2$ and $k_x = -0.7$ on a lattice of size $L_y = 30$. Varying Δ rotates the spin from $\sigma_x = -1$ towards $\sigma_z = +1$ (black arrows), matching the prediction of Eq. (27). The solid (dashed) lines correspond to finite lattice numerical (infinite lattice theory) results. (b) Spin texture along the Fermi arc at $E = 0$ for $\Delta = 0$ and 2.3 plotted with the interface spectral function at zero energy. The spin texture obtained in the infinite lattice theory via Eq. (27) (white arrows) is overlaid onto the finite lattice numerical results (blue arrows). Note that $\langle\sigma_y\rangle$ is always zero (see Appendix C).

V. CONTINUUM INTERFACE THEORY

A simplified model that can capture the effect of tunneling is a continuum model that is valid near $k_y = 0$. We note that in order to satisfy the boundary conditions at the interface, we have chosen to keep the second derivative in the y-direction, as can be seen below.

A. $\Delta = 0$

We first consider the $\Delta = 0$ case, a semi-infinite WSM slab in the continuum limit. Starting from the bulk lattice model $\mathcal{H}_w^{\text{bulk}}$ and keeping the $O(k_y^2)$ terms, we let $k_y = -i\partial_y$ and multiply by $i\sigma_y$ throughout to arrive at the differential equation (with $t = 1$):

$$\partial_y\boldsymbol{\psi} + \frac{\sigma_x}{2}\partial_y^2\boldsymbol{\psi} = i\sigma_y(E - t\sin k_x\sigma_x)\boldsymbol{\psi} + h_z\sigma_x\boldsymbol{\psi}, \tag{28}$$

where $h_z \equiv g_3 - t$. To hone in on the objective interface states, we take the interface to be at $y = 0$ and make the

Ansatz $\boldsymbol{\psi} \propto e^{\kappa y}\boldsymbol{\phi}$, where $\boldsymbol{\phi}$ is an unspecified spinor and $\mathrm{Re}(\kappa) > 0$ such that $\boldsymbol{\psi} \to 0$ as $y \to -\infty$. The differential equation (28) admits four solutions for κ, of which two have a putatively positive real part:

$$\kappa_{\pm}^2 = 2(1+h_z) \pm 2[1 + 2h_z + E^2 - \sin^2 k_x]^{\frac{1}{2}}. \tag{29}$$

For a state of energy E, $\mathrm{Re}(\kappa) > 0$ translates to $E^2 < \sin^2 k_x + h_z^2$, in agreement with the infinite lattice theory. Equation (29) sheds light on the fact that for a given eigenvector with energy E satisfying Eq. (28), there is a distinct eigenvector with equal and opposite energy $-E$ which is also a solution. Therefore, there are two κ values per energy.

To determine which solution is correct, we impose the boundary condition $\boldsymbol{\psi}(0) = 0$. In general, one has the superposition $\boldsymbol{\psi} \propto e^{\kappa_+ y}\boldsymbol{\phi}_{\kappa_+} + \alpha e^{\kappa_- y}\boldsymbol{\phi}_{\kappa_-}$. Therefore, $\alpha = -1$ and $\boldsymbol{\phi}_{\kappa_+} = \boldsymbol{\phi}_{\kappa_-}$. Equating the ratio of spinor components, the latter condition can be surmised as

$$\frac{E + h_z - \kappa_+^2/2}{\sin k_x + \kappa_+} = \frac{E + h_z - \kappa_-^2/2}{\sin k_x + \kappa_-}. \tag{30}$$

After some algebra, we recover the aforementioned chiral state of energy $E = -\sin k_x$, leading to the decay parameters $\kappa_\pm = 1 \pm \sqrt{1 + 2h_z}$ and spin in the negative x-direction:

$$\boldsymbol{\psi}_{\mathrm{chiral}} \propto e^{ik_x + ik_z z}(e^{\kappa_+ y} - e^{\kappa_- y})\begin{pmatrix} 1 \\ -1 \end{pmatrix}. \tag{31}$$

The condition of $\mathrm{Re}(\kappa) > 0$ leads once again to $\gamma < \cos k_z$, which is the familiar arc condition. At the surface BZ origin $\mathbf{k}_{\perp,0} = (0,0)$, the chiral state's decay length is on the order of a lattice length, pointing to a strongly localized state. At the surface Weyl points $\mathbf{k}_{\perp,w}^{\pm} = (0, \pm k_w)$, however, $\kappa_- = 0$ and the chiral state's decay length diverges, as expected from the absence of such surface states at the Weyl node.

B. $\Delta > 0$

To get a simple analytical result, we imagine coupling the WSM to a quantum dot of energy M. Here, we model the metal as a flat band since it is well above the WSM, and only states with the same energy are relevant. The continuum Hamiltonian reads

$$H_{\mathrm{cont}} = \begin{pmatrix} \sin k_x \sigma_x + h_z \sigma_z - i\sigma_y \partial_y - \frac{1}{2}\sigma_z \partial_y^2 & \Delta \\ \Delta & M \end{pmatrix}. \tag{32}$$

Once again, we focus on solutions bound to the interface $\boldsymbol{\psi}_w \propto e^{\kappa y}\boldsymbol{\phi}_w$ ($\boldsymbol{\psi}_m \propto e^{-\kappa_m y}\boldsymbol{\phi}_m$), leading to four differential equations. The first two restrict the metal spinors to be identical to the Weyl spinors up to a scalar factor:

$$\boldsymbol{\phi}_m = \frac{\Delta}{E - M}\boldsymbol{\phi}_w. \tag{33}$$

The remaining two equations reduce to a 2×2 matrix equation expressed in the basis of Weyl spinors $\boldsymbol{\phi}_w$:

$$\left(E - \frac{\Delta^2}{E - M} - \sin k_x \sigma_x - h_z \sigma_z + \frac{\kappa^2}{2}\sigma_z + i\kappa\sigma_y\right)\boldsymbol{\phi}_w = 0, \tag{34}$$

which is the continuum form of Eq. (19). When $\Delta = 0$ and $E \neq M$, it is not difficult to see that the bare WSM surface chiral state is recovered. For $\Delta > 0$, the physics are identical to the $\Delta = 0$ case with the substitution $E \to E - \Delta^2/(E - M) = E_\Delta$.[3] For instance, the decay parameters are now

$$\kappa_\pm^2 a^2 t = 2(t + h_z) \pm 2\left(t^2 + 2th_z - t^2 \sin^2 k_x + E_\Delta^2\right)^{\frac{1}{2}}, \tag{35}$$

where we have reinserted the energy scale t and the lattice constant a.

The continuum interface theory therefore hints at a straightforward interpretation of the energy shift upon tunneling. Indeed, seeing as the only effect of Δ was to shift the energies, the chiral band's energy in the continuum theory is defined by $E_\Delta = -t \sin k_x$, or

$$E = \frac{M - t\sin k_x}{2} - \frac{1}{2}[(M + t\sin k_x)^2 + 4\Delta^2]^{\frac{1}{2}}. \tag{36}$$

In regimes where the decay lengths $\kappa_\pm^{-1} \sim a$, Eq. (36) is in agreement with finite lattice simulations, as shown in Fig. 5. As for the chiral state's spin, it remains unchanged due to Eq. (30) still being satisfied and equal to -1 when $E \to E_\Delta = -t \sin k_x$.[4] Therefore, the validity of Eq. (36) will depend wholly on whether or not the state is in a $\sigma_x = -1$ eigenstate, and any deviations in the band structure must reflect a changing spin in the lattice model. Since the spins do in fact rotate for $\Delta \gtrsim t$, this is the root of the continuum theory's inaccuracy in this regime.

Another aspect captured by the continuum theory is the localization of bulk states at the interface to produce the emergent interface state, a typical feature of systems with boundary topologies [32]. Simply put, the lowering of energy with tunneling will give the bulk state's decay parameter a positive real part, even for arbitrarily small Δ.

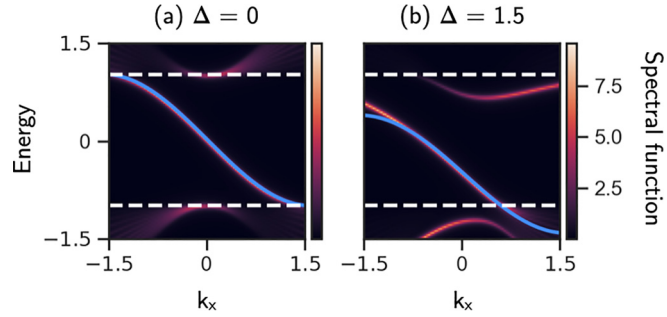

FIG. 5. Spectral function at the interface for the WSM-metal system ($L_y = 30$) at $k_z = 0$ for a tunneling strength of (a) $\Delta = 0$ and (b) $\Delta = 1.5$. The blue line is the analytic chiral state dispersion E_{chiral}, whereas the dashed white lines represent the bulk energy gap $E_{\mathrm{bulk}} = \pm 1$. The metal energy is $M = 4$.

[3] In fact, the effective surface propagator Eq. (9) exactly reduces to $-\Delta^2/(E - M)$ when $t_m = 0$ and $\mu = -M$.

[4] In the infinite lattice theory, the replacement

$$E \to E_\Delta = -t \sin k_x = -g_1$$

in Eq. (27) also leads to a spin $\sigma_x = -1$ ($\phi_w^\uparrow/\phi_w^\downarrow = 0$).

VI. TRANSPORT

We will now turn to the transport consequences of the previously described theory and numerics. We study the current along the interface (traveling in the x-direction). We fix k_z and analyze transport in 2D, summing over all momenta at the end.

At $\Delta = 0$, the conductance at the Weyl node should vanish due to the gap closure and subsequent absence of unidimensional current-carrying states. For $\Delta > 0$, however, the presence of interface states near the Weyl node and the resulting spectral asymmetry in k_x [Fig. 3(b.iii)] suggests a jump in group velocity $\partial_{k_x} E$ across the Weyl point, leading to a nonzero conductance.

We verify our reasoning numerically via the Landauer-Büttiker formalism, where conductance along the interface $\mathcal{G}_\parallel$ is defined as [33]

$$\mathcal{G}_\parallel(E) = \frac{e^2}{h}\mathrm{Tr}(G^R \Gamma_l G^A \Gamma_r). \tag{37}$$

Here, G^R is the usual retarded Green's function

$$G^R = (E - H - \Sigma^R)^{-1} \tag{38}$$

with the lead self-energy $\Sigma^R = \Sigma_l^R + \Sigma_r^R$ giving the quasiparticles a finite lifetime. The Γ_l and Γ_r operators describe the loss of electrons into the left and right leads, respectively:

$$\Gamma_{l(r)} = i\left(\Sigma^R_{l(r)} - \Sigma^A_{l(r)}\right) = -2\,\mathrm{Im}\left(\Sigma^R_{l(r)}\right). \tag{39}$$

For simplicity, we place two leads, one on each of the x-boundaries, which span the entire sample in the y-direction. Since the leads are (the interface is) in the plane perpendicular to x (y), our construction forces the sample to be open in both the x-direction and the y-direction while still remaining periodic in z. For any k_z, Σ_l^R takes the form

$$\left(\Sigma_l^R\right)_{x,x';y,y'} = -\frac{i}{2\tau}\delta_{x0}\delta_{xx'}\delta_{yy'}, \tag{40}$$

where τ is the quasiparticle's lifetime. For its part, Σ_r^R admits a similar form with $\delta_{x,0}$ replaced by δ_{x,L_x-1}. The tunneling matrix T now adopts a new diagonal sub-component in the x-direction:

$$T_{x,x';y,y'} = \Delta\delta_{xx'}\delta_{y0}\delta_{y'L_y}. \tag{41}$$

For $\Delta = 0$ [Fig. 6, panels (a) and (b), top row], the e^2/h quantized conductance for $|k_z| < k_w$ can be understood in the context of the quantum anomalous Hall effect, treating each constant k_z plane as a 2D quantum spin Hall insulator with one-dimensional edge states carrying $\mathcal{G}_\parallel = e^2/h$ [34].

At $k_z = 0$ [Fig. 6(a)], the surface tunneling, $\Delta \neq 0$, localizes a bulk state to within the gap, allowing for both left- and right-moving carriers to produce a "bump" in the conductance. One can reason by examining the juxtaposed spectrum. Above and below the bump energies (denoted by pink and green lines), there is only one left-moving state, whereas within it there are two left-movers and one right-mover. Without scattering between left- and right-movers, these states should contribute $2e^2/h$ to the conductance in one direction and e^2/h in the other direction. On the other hand, scattering may reduce the conductance since a left- and right-mover can hybridize. In our case, the scattering is provided by the leads,

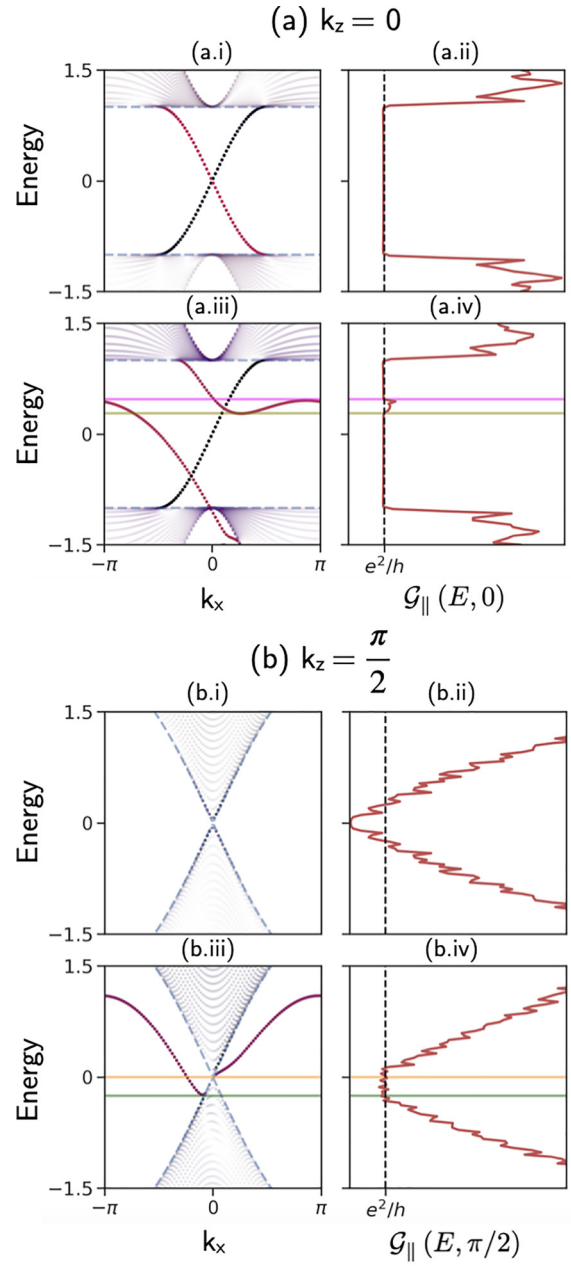

FIG. 6. Conductance $\mathcal{G}_\parallel$ of the WSM-metal system along the interface at (a) $k_z = 0$ and (b) $k_z = \pi/2$ for $\Delta = 0$ (i,ii) and $\Delta = 2.3$ (iii,iv). To guide the physical intuition, the spectra are shown in the left panels (i,iii) and states are colored and shaded according to their y-position, with the relevant interface states in dark magenta and bulk states in faint colors. Energies relevant to the discussion in Sec. VI are denoted by full horizontal lines.

and therefore the resulting conductance is between one and two quanta of conductance.

The effect of tunneling is perhaps most pronounced at the Weyl node [Fig. 6(b)]. As discussed, the bulk gap closes and the subsequent absence of interface states leads to zero conductance at zero energy when $\Delta = 0$. However, with tunneling there are now two interface states in the spectrum: The left-moving chiral state and the right-moving emergent interface state. The former will terminate at an energy E_{term}

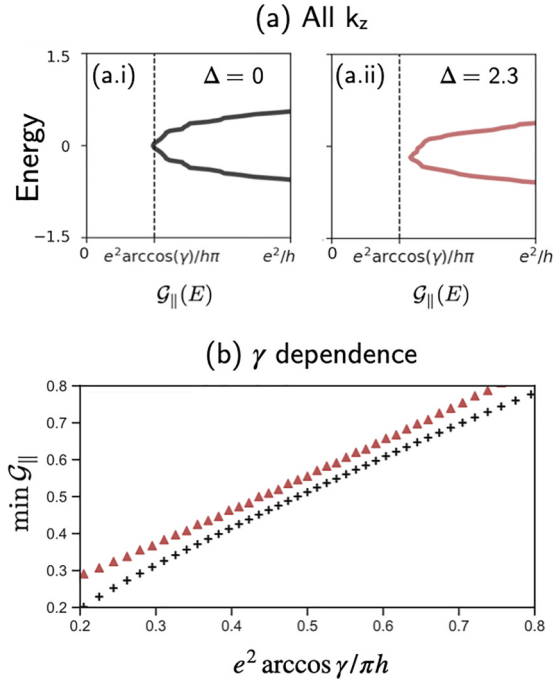

FIG. 7. (a) Conductance summed over all k_z for $\Delta = 0$ (i) and $\Delta = 2.3$ (ii). (b) Total conductance minimum (43) as a function of bare Fermi arc length. For $\Delta = 0$ (black crosses), $k^z_{\text{arc}} = 2\arccos\gamma$ and the minimum conductance scales with the Fermi arc length (modulo scattering). For $\Delta = 2.3$ (red triangles), $k^z_{\text{arc}} > 2\arccos\gamma$ and the conductance minimum is therefore increased relative to $\Delta = 0$.

(green line), the intersection of $E_{\text{bulk}} = (t^2 \sin^2 k_x + h_z^2)^{\frac{1}{2}}$ with the energy from Eq. (21). Below E_{term}, there are no unidirectional carriers and the conductance is unchanged. For $E_{\text{term}} < E < 0$, the emergent interface state is absent and the chiral state is present, so there is a conductance e^2/h per k_z slice. Note the deviation from e^2/h due to the small amount of bulk states present near zero energy. Above this range, both the chiral and the emergent interface states are present and move in opposite directions—their sum is null (modulo scattering), and only bulk states contribute.

When experimentally measuring transport between leads, the measured quantity is a sum over all k_z momenta. We therefore define the total conductance along the interface,

$$\mathcal{G}_\parallel(E) = \frac{1}{L_z}\sum_{k_z} \mathcal{G}_\parallel(E, k_z). \tag{42}$$

Summing over quantized conductance contributions on the z-projected Fermi arc k^z_{arc}, Eq. (42)'s minimum is fixed (Fig. 7):

$$\min \mathcal{G}_\parallel = \frac{e^2}{h}\frac{k^z_{\text{arc}}}{2\pi}. \tag{43}$$

To probe this signature, we vary the arc length along the k_z-direction, as shown by Fig. 7(b). In the minimal model, this can be done by applying a Zeeman coupling $b_z \mathbf{e}_z$ to spin degrees of freedom, bringing the arc length to $k^z_{\text{arc}} \to 2\arccos(\gamma + b_z)$ provided b_z is small enough not to change the overall topological phase and that its orbital effects may be neglected.

Finally, transport across the interface (i.e., traveling in the y-direction) is touched upon in Appendix D and is found to reproduce standard tunneling conductance.

VII. CONCLUSION AND DISCUSSION

Using both lattice and continuum frameworks, we have described the behavior of a $\mathcal{T}$-broken WSM's interface in proximity to a nonmagnetic band. When coupled to this band via nonmagnetic surface tunneling, the WSM's chiral state lowers in energy and forms, together with a previously delocalized bulk state, a noticeable spin-dependent asymmetry in the interface spectrum across the Weyl nodes. To model this phenomenon, we derived an infinite lattice theory of the interface and compared it to finite lattice model numerical results. We found that the infinite lattice theory accurately described the behavior of the chiral state in the entire Brillouin zone (BZ), from its energy asymmetry to the spin rotation at the interface. The localization of bulk states and the curving of the Fermi arc was also captured by the infinite lattice theory. To build intuition, we also derived a simpler continuum theory of interface states which captured the physics near $\mathbf{k}_{\perp,0}$.

Using the Landauer-Büttiker formalism, we calculated the transport of Weyl electrons traveling along the interface. Due to the asymmetry and increased Fermi arc length which allows for the presence of interface states beyond $\mathbf{k}^{\pm}_{\perp,w}$, we found a quantized increase in conductance per k_z at the Weyl nodes due to tunneling. We proposed a possible probe of this increase by relating the minimum in total conductance to the Fermi arc length.

Though this toy model described the minimal case of two Weyl nodes in a magnetic WSM with strong localized tunneling, these nodes always come in pairs connected by Fermi arcs. It is therefore reasonable to expect that the results obtained herein will still manifest themselves in more complicated systems with, e.g., broken inversion symmetry and a greater number of Fermi arcs. Finally, the asymmetry is resolved if one also accounts for the Hamiltonian's $\mathcal{T}$-reversed partner $\sigma_y H^*_w(-\mathbf{k})\sigma_y$, instead of breaking inversion symmetry.

ACKNOWLEDGMENTS

We would like to thank C.-T. Chen, A. Grushin, and B. Levitan for helpful discussions. L.G. acknowledges the hospitality of the Houches School of Physics and financial support from the NSERC CGS-M scholarship. T.P.B. acknowledges funding from NSERC and FRQNT.

APPENDIX A: THE FULL HAMILTONIAN

Recall the Hamiltonian for the full (finite-sized) system:

$$H = \sum_{\mathbf{k}_\perp} \sum_{y,y'=-L_y+1}^{L_y} \mathbf{f}^\dagger_{\mathbf{k}_\perp,y} \mathcal{H}(\mathbf{k}_\perp)_{y,y'} \mathbf{f}_{\mathbf{k}_\perp,y'}, \tag{A1a}$$

$$\mathcal{H}(\mathbf{k}_\perp) = \begin{pmatrix} \mathcal{H}^{\text{open}}_w(\mathbf{k}_\perp) & T^\dagger \\ T & \mathcal{H}^{\text{open}}_m(\mathbf{k}_\perp) \end{pmatrix}, \tag{A1b}$$

where

$$\mathbf{f}_{\mathbf{k}_\perp,y} = \begin{cases} \mathbf{c}_{\mathbf{k}_\perp,y}, & -L_y + 1 \leqslant y \leqslant 0, \\ \mathbf{d}_{\mathbf{k}_\perp,y}, & 1 \leqslant y \leqslant L_y, \end{cases} \tag{A2}$$

with $\mathbf{c}_y = (c_{\mathbf{k}_\perp,y,\uparrow}, c_{\mathbf{k}_\perp,y,\downarrow})^\top$. $\mathcal{H}^{\text{open}}$ is the partial-in-y Fourier transform of $\mathcal{H}^{\text{bulk}}$. There is translational invariance in both x and z, so each block is in general a function of $\mathbf{k}_\perp$.

The bare Weyl Hamiltonian $\mathcal{H}_w^{\text{open}}$ is

$$\mathcal{H}_w^{\text{open}} = \mathbf{C}_0 \otimes \mathbf{h}_w + \mathbf{C}_1 \otimes \mathbf{R}_w + \mathbf{C}_1^\dagger \otimes \mathbf{R}_w^\dagger, \tag{A3}$$

where $\mathbf{C}_0$ is the L_y-sized identity and $(\mathbf{C}_1)_{y,y'} = \delta_{y+1,y'}$ is the displacement operator on the lattice. Here,

$$\mathbf{h}_w = t_x \sin k_x \sigma_x + t_z(2 + \gamma - \cos k_x - \cos k_z)\sigma_z, \tag{A4a}$$

$$\mathbf{R}_w = \frac{it_y}{2}\sigma_y - \frac{t_z}{2}\sigma_z \tag{A4b}$$

are the spin-matrices corresponding to same-site and nearest-neighbor hopping, respectively.

The bare metal Hamiltonian $\mathcal{H}_m^{\text{open}}$ is written in a similar form ($\mathbb{1}$ is the identity matrix in spin):

$$\mathcal{H}_m^{\text{open}} = h_m \mathbf{C}_0 \otimes \mathbb{1} - t_m \mathbf{C}_1 \otimes \mathbb{1} - t_m \mathbf{C}_1^\dagger \otimes \mathbb{1} \tag{A5}$$

with

$$h_m = -2t_m(\cos k_x + \cos k_z) - \mu. \tag{A6}$$

APPENDIX B: THE INTERFACE SPECTRUM FOR DIFFERENT BAND CONFIGURATIONS

The asymmetry at the Weyl node illustrated in Fig. 3(b) is also apparent for different choices of μ, t_m, and metal band structure. To convince ourselves of our specific model's ubiquitous features, we display a few more metal configurations in Fig. 8(a). We expect that in the more realistic setup of a WSM coupled to a two-band bulk insulator, both copies will be present: One for positive and one for negative energies. This is confirmed in what follows.

One may also imagine coupling the WSM to a two-band bulk insulator, i.e., two copies of the single bulk metal band separated by a gap. Keeping each individual band nonmagnetic, the Hamiltonian is now

$$H = \begin{pmatrix} \mathcal{H}_w^{\text{open}} & T^\dagger & T^\dagger \\ T & \mathcal{H}_+^{\text{open}} & 0 \\ T & 0 & \mathcal{H}_-^{\text{open}} \end{pmatrix}, \tag{B1}$$

where $\mathcal{H}_\pm^{\text{open}}$ represent the metal Hamiltonian $\mathcal{H}_m^{\text{open}}$ with parameters $t_{m,\pm} = \pm t_m$, $\mu_\pm = \pm\mu$, and T is the same as before. The resulting spectrum is shown in Fig. 8(b). Unsurprisingly, we recover two copies of the previously observed, single-band asymmetry: One for positive energies and one for negative energies. The asymmetry is therefore resolved if one inverts both the momentum and the energy.

Though the case of a band with zero bandwidth $t_m = 0$ is not physically realistic, it still reproduces the same qualitative asymmetry. For mathematical simplification, therefore, we may set $t_m = 0$ as is done in the continuum theory and spin rotation discussion. We ultimately choose to work with $\mu = -4$ and $t_m = 0.5$ and a single metal band due to the clear asymmetry across the Weyl node and separation between bulk WSM and metal dispersions.

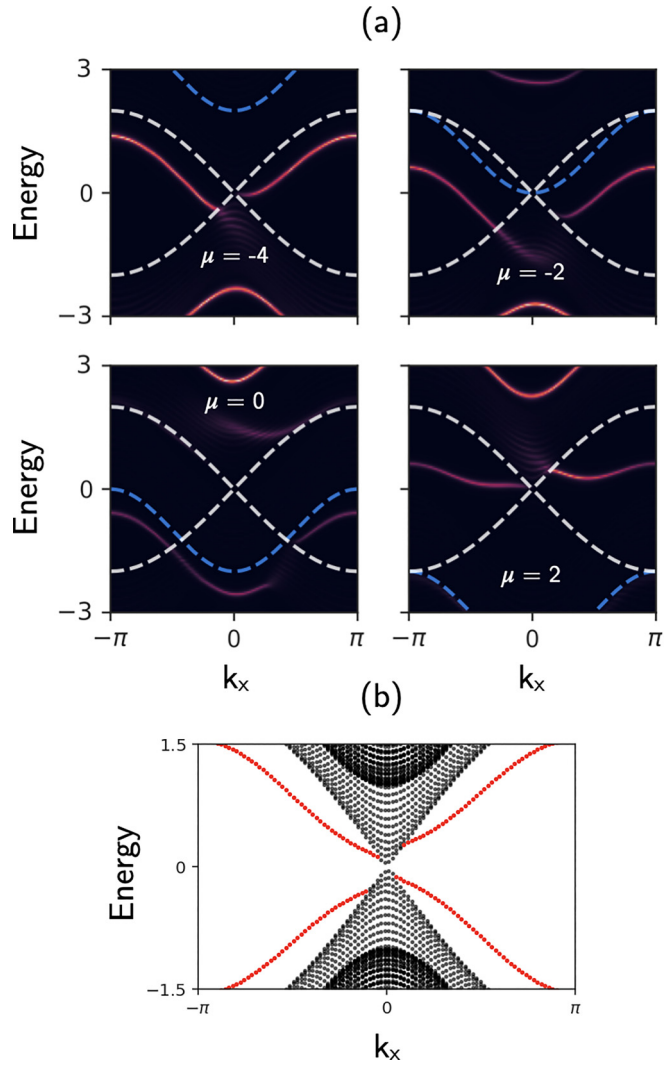

FIG. 8. The energies at the Weyl node for various parabolic band configurations at $\Delta = 2.3$. (a) The interface spectral function for $t_m = 0.5$ at (from left to right, top to bottom) $\mu = -4$, -2, 0, and $+2$ as defined by Eq. (4). The WSM (metal) bulk edge is shown by dashed white (blue) lines. (b) The band structure for a WSM in contact with the two-band insulator [Eq. (B1)]. States localized to the interface are shown in red.

APPENDIX C: $\langle\sigma_y\rangle = 0$ IN AN OPEN WSM

In the bulk, it is clear that $\langle\sigma_y\rangle$ may be any value. In particular, the spin-orbit coupling in a Weyl Hamiltonian of the form $\mathbf{k}\cdot\boldsymbol{\sigma}$ will tie the y-momentum k_y to the spin in that same direction. Upon opening our system in the y-direction, however, $\langle\sigma_y\rangle = 0$ identically throughout. Similarly, opening the system in x renders $\langle\sigma_x\rangle = 0$.

One can see why this is the case by examining the finite-sized WSM Hamiltonian Eq. (A3). Written in matrix form, the

blocks are

$$\mathbf{h}_w = \begin{pmatrix} g_3 & g_1 \\ g_1 & -g_3 \end{pmatrix}, \tag{C1a}$$

$$\mathbf{R}_w^\dagger = \frac{1}{2}\begin{pmatrix} -t_z & t_y \\ -t_y & t_z \end{pmatrix} \tag{C1b}$$

in spin space, where $t_{x,y,z}$ are real. Adding these blocks into the finite-sized matrix H_w leads to a real and Hermitian (or symmetric) matrix, i.e., $H_w^\top = H_w$. We set out to prove that one can always find real eigenstates to a real symmetric matrix, thereby rendering $\langle\sigma_y\rangle = 0$ identically as σ_y is purely imaginary.

To prove this, we start by noting that the eigenvalues of a symmetric matrix are real. Now, take $H_w|\psi\rangle = E|\psi\rangle$. Adding it to its complex conjugate yields

$$H_w(|\psi\rangle + |\psi\rangle^*) = E(|\psi\rangle + |\psi\rangle^*). \tag{C2}$$

Now, if $|\psi\rangle = -|\psi\rangle^*$ then $|\psi\rangle$ is purely imaginary and we can therefore define $|\psi\rangle = i|\varphi\rangle$ with $|\varphi\rangle$ purely real, satisfying $H_w|\varphi\rangle = E|\varphi\rangle$. Otherwise, if $|\psi\rangle + |\psi\rangle^* \neq 0$ then it is necessarily real. Therefore, one may always find a complete set of real eigenvectors to a real symmetric matrix. Since the eigenvectors are purely real and the matrix σ_y contains only imaginary entries,

$$\langle\psi|\sigma_y|\psi\rangle = 0. \tag{C3}$$

Of course, one can always perform a unitary rotation in spin space such that $\sigma_x \to \sigma_y$ and $\sigma_y \to -\sigma_x$. In this case, an open system in x exactly mirrors one open in y before the rotation, and $\langle\sigma_x\rangle = 0$ likewise follows. One should note that in the case of degeneracies (such as bulk states with the same energy at k_y and $-k_y$), it is possible to construct a superposition of states that have a nonzero σ_y value. Surface states, however, have no such degeneracy and are therefore guaranteed to have a zero spin in the y-direction.

APPENDIX D: DERIVATION OF CONDUCTANCE ACROSS THE INTERFACE

We set out to derive an expression for the conductance across the interface $\mathcal{G}_{\perp,\sigma} = dI_\sigma/dV$ of a particle polarized with spin σ. We begin by expressing the current I_σ of a particle with spin σ in terms of the retarded correlation function $U_R^{\sigma\sigma'}$ [35–37]:

$$I_\sigma = -2e\,\mathrm{Im}\sum_{\sigma'} U_R^{\sigma\sigma'}(-eV). \tag{D1}$$

$U_R^{\sigma\sigma'}(-eV)$ is found by computing the Matsubara correlation function $\mathcal{U}^{\sigma\sigma'}(i\omega_n)$ and analytically continuing $i\omega_n \to -eV + i0^+$. At finite temperature β^{-1}, we have

$$\mathcal{U}^{\sigma\sigma'}(i\omega_n) = \frac{1}{\beta}\sum_{\mathbf{kq}} |T_{\mathbf{kq}}|^2 \sum_{ip} g_w^{\sigma'\sigma}(\mathbf{k}, ip - i\omega_n) g_m^{\sigma\sigma'}(\mathbf{q}, ip), \tag{D2}$$

where $\mathbf{k}$ ($\mathbf{q}$) is the momentum in the WSM (metal), $T_{\mathbf{kq}}$ is the tunneling matrix element, ω_n (p) is a bosonic (fermionic) Matsubara frequency, and $\boldsymbol{g}_w$ ($\boldsymbol{g}_m$) is the Matsubara Green's function for the bare WSM (metal). Since states bound to the interface will not contribute to tunneling across from it, we may consider only bulk states. The bulk Green's functions $\boldsymbol{g}_{m,w}$ are therefore

$$\boldsymbol{g}_m(\mathbf{q}, ip) = \frac{1}{ip - \xi_m}, \tag{D3a}$$

$$\boldsymbol{g}_w(\mathbf{k}, ip) = \frac{ip + \mathcal{H}_w^{\mathrm{bulk}}}{(ip - \xi_w)(ip + \xi_w)}, \tag{D3b}$$

with the WSM (metal) dispersion ξ_w (ξ_m). Setting $|T_{\mathbf{kq}}|^2 = \Delta^2\delta(\mathbf{k}_\perp - \mathbf{q}_\perp)$, we perform the Matsubara frequency summation $\sum_{ip}(ip - \xi)^{-1} = \beta n_F(\xi)$ [36], where n_F is the fermionic distribution, by splitting the denominator into partial fractions. Using $\mathrm{Im}\,(-eV + i0^+ - \xi)^{-1} = -\pi\delta(-eV - \xi)$, Eq. (D1) becomes

$$I = 2e\Delta^2 \sum_{\mathbf{k}_\perp, k_y, q_y} \big\{u_{\mathbf{k}}^2[n_F(\xi_m) - n_F(\xi_w)]\delta(-eV - \xi_-) + v_{\mathbf{k}}^2[n_F(\xi_m) - n_F(-\xi_w)]\delta(-eV - \xi_+)\big\}, \tag{D4}$$

where $\xi_\pm = \xi_m \pm \xi_w$ and

$$u_{\mathbf{k}}^2 = \tfrac{1}{2}(1 + t\sin k_x/\xi_w), \tag{D5a}$$

$$v_{\mathbf{k}}^2 = \tfrac{1}{2}(1 - t\sin k_x/\xi_w). \tag{D5b}$$

Note that we have chosen the quantization axis in the x-direction for simplicity. More generally, the second term in Eqs. (D5) is an odd function of k_x, k_z, and ξ_w and will vanish when integrated over, leaving the current spin-independent.

Equation (D4) has two terms: The first (second) corresponds to tunneling from the upper (lower) WSM band to the metal band. Each term has three parts: The Dirac δ imposes energy conservation, $n_F(\xi_m) - n_F(\xi_w)$ counts the participating states available to tunnel, while $u_{\mathbf{k},\sigma}^2$ and $v_{\mathbf{k},\sigma}^2$ weigh the bands according to their corresponding spin. All of this is proportional to Δ^2, the amplitude of a tunneling interaction in light of the exact action Eq. (8).

To proceed, we imagine placing the metal band's Fermi level μ_m in the WSM's upper band and largely above the parabolic band minimum. At low energies,

$$\xi_w = v\big(\mathbf{k}_\perp^2 + k_y^2\big)^{\frac{1}{2}} \tag{D6a}$$

and

$$\xi_m = \mu_m + \frac{1}{m}\big(2m\tilde{\mu} - \mathbf{k}_\perp^2\big)^{\frac{1}{2}} q_y, \tag{D6b}$$

where $m = 1/2t_m$ and $\tilde{\mu} = \mu + \mu_m + 6t_m$ (the lattice constant is still $a = 1$). The latter expression is found by expanding near ξ_m's intercept with μ_m along q_y, the metal's y-momentum. We further consider a small positive applied voltage such that particles tunnel from the upper WSM band to the metal. Thus, only the first term of Eq. (D4) contributes. Replacing the sums by integrals, changing variables from k_y to ξ_w and q_y to ξ_m, and reinserting $\hbar$, the current is now

$$I = \frac{e}{h}\frac{m\Delta^2}{2\pi v^2}\int_0^{eV} d\xi_w \int \frac{d^2\mathbf{k}_\perp}{(2\pi)^2}\xi_w u_{\mathbf{k}}^2 \times \frac{\theta(\xi_w - v|\mathbf{k}_\perp|)\theta(2m\tilde{\mu} - \mathbf{k}_\perp^2)}{\sqrt{\xi_w^2/v^2 - \mathbf{k}_\perp^2}\sqrt{2m\tilde{\mu} - \mathbf{k}_\perp^2}}. \tag{D7}$$

Note that we have applied the low-temperature limit $n_F(\xi_w) = \theta(-\xi_w)$. The integral over $d^2\mathbf{k}_\perp$ can be done analytically, yielding the conductance across the interface:

$$\mathcal{G}_\perp(eV) = \frac{e^2}{h}\frac{m\Delta^2}{(2\pi)^2 v^2} eV \log\left|\frac{\varepsilon + eV}{\varepsilon - eV}\right|. \tag{D8}$$

For $eV \ll \sqrt{2mv^2\tilde{\mu}} \equiv \varepsilon$, the leading-order term is quadratic in V:

$$\mathcal{G}_\perp(eV) \approx \frac{e^2}{h}\frac{2m\Delta^2}{(2\pi)^2 v^2 \varepsilon}(eV)^2. \tag{D9}$$

Equation (D9) maintains that tunneling measurements with featureless metals reveal the density of states at the tunneling energy, since the three-dimensional WSM's linear dispersion corresponds to a density of states proportional to E^2.

[1] N. P. Armitage, E. J. Mele, and A. Vishwanath, Weyl and Dirac semimetals in three-dimensional solids, Rev. Mod. Phys. **90**, 015001 (2018).

[2] S.-Q. Shen, *Topological Insulators: Dirac Equation In Condensed Matters* (Springer, Singapore, 2012).

[3] B. Bernevig, It's been a Weyl coming, Nature (London) **11**, 698 (2015).

[4] S.-Y. Xu, I. Belopolski, N. Alidoust, M. Neupane, G. Bian, C. Zhang, R. Sankar, G. Chang, Z. Yuan, C.-C. Lee, S.-M. Huang, H. Zheng, J. Ma, D. S. Sanchez, B. Wang, A. Bansil, F. Chou, P. P. Shibayev, H. Lin, S. Jia *et al.*, Discovery of a Weyl fermion semimetal and topological Fermi arcs, Science **349**, 613 (2015).

[5] M. Hasan, G. Chang, I. Belopolski, G. Bian, S.-Y. Xu, and J.-X. Yin, Weyl, Dirac and high-fold chiral fermions in topological quantum matter, Nat. Rev. Mater. **6**, 784 (2021).

[6] S.-Y. Xu, N. Alidoust, I. Belopolski, Z. Yuan, G. Bian, T.-R. Chang, H. Zheng, V. N. Strocov, D. S. Sanchez, G. Chang, C. Zhang, D. Mou, Y. Wu, L. Huang, C.-C. Lee, S.-M. Huang, B. Wang, A. Bansil, H.-T. Jeng, T. Neupert *et al.*, Discovery of a Weyl fermion state with Fermi arcs in niobium arsenide, Nature (London) **11**, 748 (2015).

[7] D. F. Liu, A. J. Liang, E. K. Liu, Q. N. Xu, Y. W. Li, C. Chen, D. Pei, W. J. Shi, S. K. Mo, P. Dudin, T. Kim, C. Cacho, G. Li, Y. Sun, L. X. Yang, Z. K. Liu, S. S. P. Parkin, C. Felser, and Y. L. Chen, Magnetic Weyl semimetal phase in a Kagomé crystal, Science **365**, 1282 (2019).

[8] A. A. Soluyanov, D. Gresch, Z. Wang, Q. Wu, M. Troyer, X. Dai, and B. A. Bernevig, Type-II Weyl semimetals, Nature (London) **527**, 495 (2015).

[9] Y. Sun, S.-C. Wu, M. N. Ali, C. Felser, and B. Yan, Prediction of Weyl semimetal in orthorhombic $MoTe_2$, Phys. Rev. B **92**, 161107(R) (2015).

[10] Y. Yoshimura, W. Onishi, K. Kobayashi, T. Ohtsuki, and K.-I. Imura, Comparative study of Weyl semimetal and topological/Chern insulators: Thin-film point of view, Phys. Rev. B **94**, 235414 (2016).

[11] A. A. Burkov, Topological properties of Dirac and Weyl semimetals, Ref. Module Mater. Sci. Mater. Eng. **1**, 2 (2022).

[12] C. Herring, Accidental degeneracy in the energy bands of crystals, Phys. Rev. **52**, 365 (1937).

[13] H. B. Nielsen and M. Ninomiya, The Adler-Bell-Jackiw anomaly and Weyl fermions in a crystal, Phys. Lett. B **130**, 389 (1983).

[14] H. B. Nielsen and M. Ninomiya, Absence of neutrinos on a lattice: (I). Proof by homotopy theory, Nucl. Phys. B **185**, 20 (1981).

[15] H. B. Nielsen and M. Ninomiya, Absence of neutrinos on a lattice: (II). intuitive topological proof, Nucl. Phys. B **193**, 173 (1981).

[16] H. B. Nielsen and M. Ninomiya, A no-go theorem for regularizing chiral fermions, Phys. Lett. B **105**, 219 (1981).

[17] A. A. Burkov, M. D. Hook, and L. Balents, Topological nodal semimetals, Phys. Rev. B **84**, 235126 (2011).

[18] A. A. Burkov and L. Balents, Weyl Semimetal in a Topological Insulator Multilayer, Phys. Rev. Lett. **107**, 127205 (2011).

[19] P. Hosur and X. Qi, Recent developments in transport phenomena in Weyl semimetals, C. R. Phys. **14**, 857 (2013).

[20] K.-Y. Yang, Y.-M. Lu, and Y. Ran, Quantum hall effects in a Weyl semimetal: Possible application in pyrochlore iridates, Phys. Rev. B **84**, 075129 (2011).

[21] X. Wan, A. M. Turner, A. Vishwanath, and S. Y. Savrasov, Topological semimetal and fermi-arc surface states in the electronic structure of pyrochlore iridates, Phys. Rev. B **83**, 205101 (2011).

[22] F. Buccheri, R. Egger, and A. De Martino, Transport, refraction, and interface arcs in junctions of Weyl semimetals, Phys. Rev. B **106**, 045413 (2022).

[23] M. Breitkreiz and P. W. Brouwer, Fermi-Arc Metals, Phys. Rev. Lett. **130**, 196602 (2023).

[24] F. Abdulla, S. Rao, and G. Murthy, Fermi arc reconstruction at the interface of twisted Weyl semimetals, Phys. Rev. B **103**, 235308 (2021).

[25] R. Kundu, H. A. Fertig, and A. Kundu, Broken symmetry and competing orders in Weyl semimetal interfaces, Phys. Rev. B **107**, L041402 (2023).

[26] G. Murthy, H. A. Fertig, and E. Shimshoni, Surface states and arcless angles in twisted Weyl semimetals, Phys. Rev. Res. **2**, 013367 (2020).

[27] N. A. Lanzillo, U. Bajpai, I. Garate, and C.-T. Chen, Size-Dependent Grain-Boundary Scattering in Topological Semimetals, Phys. Rev. Appl. **18**, 034053 (2022).

[28] J. Borchmann and T. Pereg-Barnea, Quantum oscillations in Weyl semimetals: A surface theory approach, Phys. Rev. B **96**, 125153 (2017).

[29] D. J. J. Marchand and M. Franz, Lattice model for the surface states of a topological insulator with applications to magnetic and exciton instabilities, Phys. Rev. B **86**, 155146 (2012).

[30] E. V. Gorbar, V. A. Miransky, I. A. Shovkovy, and P. O. Sukhachov, Surface Fermi arcs in $\mathbb{Z}_2$ Weyl semimetals A_3Bi (A = Na, K, Rb), Phys. Rev. B **91**, 235138 (2015).

[31] A. Potter, I. Kimchi, and A. Vishwanath, Quantum oscillations from surface Fermi arcs in Weyl and Dirac semimetals, Nat. Commun. **5**, 5161 (2014).

[32] T. Pereg-Barnea and H.-H. Lin, Andreev edge state on semi-infinite triangular lattice: Detecting the pairing symmetry in $Na_{0.35}CoO_2 \cdot yH_2O$, Europhys. Lett. **69**, 791 (2005).

[33] S. Datta, *Electronic Transport in Mesoscopic Systems*, Cambridge Studies in Semiconductor Physics and Microelectronic Engineering (Cambridge University Press, Cambridge, 1995).

[34] B. A. Bernevig, T. L. Hughes, and S.-C. Zhang, Quantum spin Hall effect and topological phase transition in HgTe quantum wells, Science **314**, 1757 (2006).

[35] M. H. Cohen, L. M. Falicov, and J. C. Phillips, Superconductive Tunneling, Phys. Rev. Lett. **8**, 316 (1962).

[36] G. D. Mahan, *Many-Particle Physics (Physics of Solids and Liquids)*, 3rd ed. (Springer, New York, 2000).

[37] D. Ryndyk, *Theory of Quantum Transport at Nanoscale*, Springer Series in Solid-State Sciences (Springer, Cham, 2016).